

# Agile Actions with a Centaur-Type Humanoid: A Decoupled Approach

Matteo Parigi Polverini, Enrico Mingo Hoffman, Arturo Laurenzi, and Nikos G. Tsagarakis

**Abstract**—The kinematic features of a centaur-type humanoid platform, combined with a powerful actuation, enable the experimentation of a variety of agile and dynamic motions. However, the higher number of degrees-of-freedom and the increased weight of the system, compared to the bipedal and quadrupedal counterparts, pose significant research challenges in terms of computational load and real implementation. To this end, this work presents a control architecture to perform agile actions, conceived for torque-controlled platforms, which decouples for computational purposes offline optimal control planning of lower-body primitives, based on a template kinematic model, and online control of the upper-body motion to maintain balance. Three stabilizing strategies are presented, whose performance is compared in two types of simulated jumps, while experimental validation is performed on a half-squat jump using the CENTAURO robot.

## I. INTRODUCTION

The problem of realizing agile and dynamic actions with a legged robotic platform is an active research topic spanning: fast dynamic gaits [1], [2], jumping [3], [4], kicking [5]. In this respect, remarkable demonstrators have been realized thanks to the recent technological advances in designing powerful, robust and increasingly lightweight robotic platforms. The seminal work of Raibert on the one-legged hopper [6], followed by the jumping and landing pneumatic robot Mowgli [7], represent the first examples of actuated jumping mechanisms. From then on, research on agile motions have been carried out, almost in parallel, on bipeds and quadrupeds. Regarding the former type of platforms, Boston Dynamics has shown Atlas running outdoor and performing the world-famous back-flip and parkour demonstrators. Implementation details have not been made available, however in [8] an algorithm is presented which combines a simplified dynamic model with the robot full kinematics to make Atlas jump in simulation. As shown in a popular video, Honda Asimo has been capable of running and performing small jumps, even on single stance, while the small-size biped QRIO, manufactured by SONY, was able to run and jump through generation of dynamically consistent motion patterns [1]. In [9] an approach based on ground reaction forces is introduced to make the HRP-2 robot perform vertical jumps in simulations. Recently, in [10] a torque and velocity controllers to perform jumps have been tested on the humanoid robot iCub. Almost concurrently, impressive results have been achieved among the quadrupedal robotic community. In

[2] the ANYmal predecessor, the StarlETH quadruped using series elastic actuators, was able to perform dynamic gaits and a squat jump. Similar results have been demonstrated on ANYmal [3] by setting user-defined base target positions to the whole-body controller in order to perform the jump. Thanks to recent advances in actuator development, pseudo-direct-drive concepts have found application in high-dynamic legged robots as in the MIT Cheetah [11], [12], which is able to run and jump at high speeds. Similar concepts have been adopted in the small-size quadrupeds Minitaur [13] and MIT Mini Cheetah [4].

## II. DECOUPLED ARCHITECTURE FOR CENTAUR-TYPE HUMANOIDS

Centaur-type humanoids, as the wheeled-legged system CENTAURO [14], represent a new kinematic paradigm that combines the inherent stability advantage of quadrupeds over bipeds, with the loco-manipulation capabilities enabled by a humanoid upper-body. In this respect, while several agile actions are theoretically enabled by such topology (if combined with a powerful actuation), the increased weight of the system and the higher number of degrees-of-freedom (DoF), compared to the bipedal and quadrupedal counterparts, pose significant research challenges. Targeting the actual realization of dynamic behaviours on a centaur-type humanoid while meeting computational and implementation requirements, we present a control architecture, designed for torque-controlled platforms, which builds upon our previous work in [15]. It consists of the following components, organized in a *decoupled* structure, see Fig. 1:

- Offline stage: a *lower-body planner* employs optimal control, applied to a quadrupedal template kinematic model, to generate a database of lower-body agile primitives, consisting in a time series of planned contact positions  $\bar{\mathbf{r}}_C \in \mathbb{R}^{k \times N_s}$  and contact forces  $\bar{\mathbf{F}}_C \in \mathbb{R}^{k \times N_s}$ . We will hereafter assume  $n_C$  point contacts, thus  $k = 3n_C$ , while  $N_s \in \mathbb{R}$  is the number of shooting intervals.
- Online stage: the planned lower-body actions are re-played on the system using upper-body motions to maintain balance. The following components are employed:
  - 1) *Upper-body stabilizer*: is responsible to maintain the balance of the whole system through upper-body motions, based on IMU angular velocity  $\boldsymbol{\omega}_{\text{imu}} \in \mathbb{R}^3$  feedback;
  - 2) *Hierarchical Inverse Kinematics (IK)*: tracks the planned lower-body contact positions  $\bar{\mathbf{r}}_C$  and the upper-body stabilizing action by means of Quadratic Programming (QP);

This work was supported by the European Union's Horizon 2020 Research and Innovation Program under Grant No. 779963 (EUROBENCH).

The authors are with the Humanoids & Human Centered Mechatronics Research Line (HHCM), Istituto Italiano di Tecnologia (IIT), Genova, Italy {matteo.parigi, enrico.mingo, arturo.laurenzi, nikos.tsagarakis}@iit.it

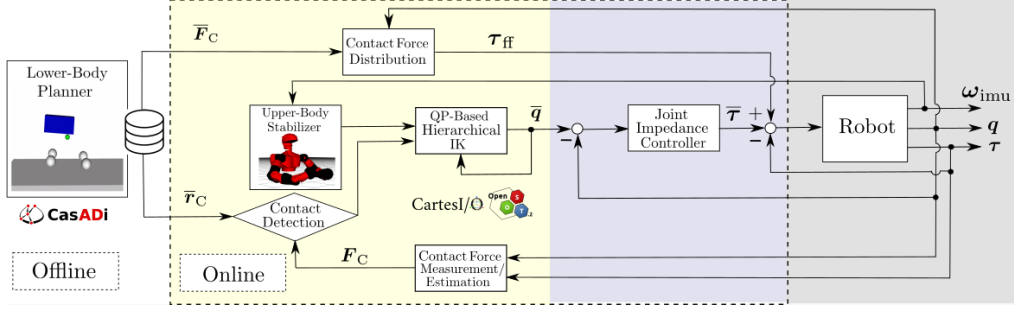


Fig. 1. Overview of the proposed decoupled architecture.

- 3) *Contact force distribution*: tracks at best the planned contact forces, while ensuring balance.
- 4) *Contact detection*: detects if contact with the environment has been established, based on estimated or measured contact forces  $F_C \in \mathbb{R}^k$ .
- 5) *Joint-level control*: a decentralized joint impedance controller with torque feed-forward  $\tau_{ff} \in \mathbb{R}^n$ , feeding the torque control loop.

While the lower-body planner and the upper-body stabilizer, which are main contributions of this paper, will be described in Sec. III and Sec. IV, respectively, the reader can refer to [15] for details on the remaining components.

### III. PLANNING LOWER-BODY ACTIONS

#### A. Lower-Body Template Kinematic Model

In order to overcome the computational complexity introduced by the adoption of a full kinematic model, the quadrupedal lower-body of a centaur-type platform will be herein modeled as a template 5-mass floating-base system. Note that, while this modelling choice simplifies the robot kinematics for computational purposes, no further simplification will be introduced on the dynamic model. With reference to Fig. 2, let us consider a floating-base system consisting of the actuated *prismatic* joint coordinates  $q_C \in \mathbb{R}^k$ , enabling the positioning of the 4 leg end-effectors. Again, as a common assumption for quadrupeds, point contacts are considered, thus  $k = 12$ . The corresponding Cartesian positions and contact forces for the  $i$ -th leg, expressed w.r.t. the world frame  $\mathcal{W}$ , are denoted with  $p_{C,i}(q) \in \mathbb{R}^3$  and  $F_{C,i} \in \mathbb{R}^3$ , respectively. The pose of the under-actuated floating-base is modeled through three prismatic joints  $p_u \in \mathbb{R}^3$  and a spherical joint, whose orientation is given by the unit quaternion  $\rho_u \in \mathbb{R}^4$ . As shown in Fig. 2, the inertial properties of each rigid body are given by the related mass value and inertia tensor. Note also that, in order to account for the presence of the robot upper-body, as in CENTAURO, the waist body mass has been shifted towards the front legs. Finally, let us consider a generic environment plane  $\mathcal{S}$ , whose orientation is given by its normal  $n_S \in \mathbb{R}^3$ . By now denoting with  $n$  and  $n_u$  the number of actuated and unactuated degrees-of-freedom (DoFs), respectively, the generalized coordinates can be collected in the vector  $q \in \mathbb{R}^{n+n_u}$ , with  $n = k$  and

$n_u = 7$  for the introduced template model:

$$q = [p_u^T \quad \rho_u^T \quad q_C^T]^T \quad (1)$$

while the generalized velocities  $\nu \in \mathbb{R}^{n+n_u-1}$  and accelerations  $\dot{\nu} \in \mathbb{R}^{n+n_u-1}$  are given by:

$$\nu = [\dot{p}_u^T \quad \omega_u^T \quad \dot{q}_C^T]^T \quad (2a)$$

$$\dot{\nu} = [\ddot{p}_u^T \quad \dot{\omega}_u^T \quad \ddot{q}_C^T]^T \quad (2b)$$

where  $\dot{p}_u, \ddot{p}_u \in \mathbb{R}^3$  and  $\omega_u, \dot{\omega}_u \in \mathbb{R}^3$  are the linear and angular velocity and acceleration, respectively, of the robot floating-base expressed in the world  $\mathcal{W}$  coordinates. Given  $\rho_u = [\epsilon_u^T \quad \eta_u]^T$ , with  $\epsilon_u \in \mathbb{R}^3$  and  $\eta_u \in \mathbb{R}$ , the quaternion propagation [16] is given by:

$$\dot{\rho}_u = \left[ \frac{1}{2} \omega_u, 0 \right] \circ \rho_u \quad (3)$$

expressing the relation between  $\dot{\rho}_u$  and  $\omega_u$ . The symbol  $\circ$  is used to denote the quaternion product.

#### B. Floating-Base Dynamic Model

The dynamics of a floating-base robot is expressed by the following equation:

$$B(q)\dot{\nu} + h(q, \nu) = S\tau + J_C^T(q)F_C \quad (4)$$

where  $\tau \in \mathbb{R}^n$  are the actuated joint torques, while  $B(q) \in \mathbb{R}^{(n+n_u-1) \times (n+n_u-1)}$  is the full joint space inertia matrix and  $h(q, \nu) \in \mathbb{R}^{n+n_u-1}$  is the vector of non-linear (gravity, centrifugal/Coriolis) terms. Differently from a fixed-base robot, the actuation matrix  $S \in \mathbb{R}^{(n+n_u-1) \times n}$  models

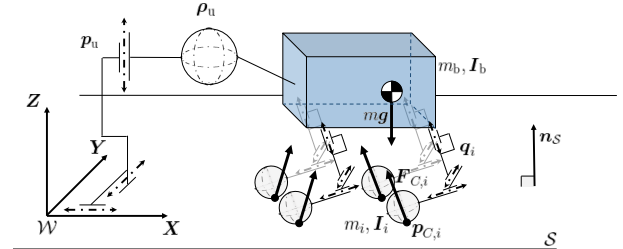


Fig. 2. The 5-mass template model for the quadrupedal lower-body featuring prismatic joints.

the system under-actuation. Contact forces  $\mathbf{F}_C \in \mathbb{R}^k$  are taken into account by concatenating the Jacobian of all support links  $\mathbf{J}_C(\mathbf{q}) \in \mathbb{R}^{k \times (n+n_u-1)}$  and the corresponding overall contact wrench. The equation of motion in (4) can be further split into  $n_u$  under-actuated and  $n$  actuated rows, denoted with subscript  $u$  and  $a$ , respectively.

$$\mathbf{B}_u(\mathbf{q})\dot{\boldsymbol{\nu}} + \mathbf{h}_u(\mathbf{q}, \boldsymbol{\nu}) = \mathbf{J}_{C,u}^T(\mathbf{q})\mathbf{F}_C \quad (5a)$$

$$\mathbf{B}_a(\mathbf{q})\dot{\boldsymbol{\nu}} + \mathbf{h}_a(\mathbf{q}, \boldsymbol{\nu}) = \boldsymbol{\tau} + \mathbf{J}_{C,a}^T(\mathbf{q})\mathbf{F}_C \quad (5b)$$

### C. Optimal Control Formulation and Transcription

Let us consider the following choice for the state  $\mathbf{x}(t)$  and control  $\mathbf{u}(t)$  vectors:

$$\mathbf{x} = [\mathbf{q}^T \quad \boldsymbol{\nu}^T]^T \quad (6a)$$

$$\mathbf{u} = [\dot{\boldsymbol{\nu}}^T \quad \mathbf{F}_C^T]^T \quad (6b)$$

Based on the floating-base model described in Sec. III-B, the OCP formulation we address in this Section reads as:

$\min_{\mathbf{x}(\cdot), \mathbf{u}(\cdot)} \int_0^T L(\mathbf{x}(t), \mathbf{u}(t)) dt + E(\mathbf{x}(T)) \quad (7)$	
subject to	
$\mathbf{x}_0 - \mathbf{x}^{\text{init}} = \mathbf{0}$	initial state
$\mathbf{x}(T) - \mathbf{x}^{\text{goal}} = \mathbf{0}$	final state
$\dot{\mathbf{x}}(t) - \mathbf{f}(\mathbf{x}(t), \mathbf{u}(t)) = \mathbf{0}$	double integrator
$\boldsymbol{\tau}_u(\mathbf{x}(t), \mathbf{u}(t)) = \mathbf{0}$	under-actuation
$\underline{\boldsymbol{\tau}} \leq \boldsymbol{\tau}(\mathbf{x}(t), \mathbf{u}(t)) \leq \bar{\boldsymbol{\tau}}$	torque bounds
$\underline{\mathbf{p}}_{Ci} \leq \mathbf{p}_{Ci}(t) \leq \bar{\mathbf{p}}_{Ci}$	work-space bounds
if $C_i$ in contact:	
$\mathbf{p}_{Ci}(t \in T_C) \in \mathcal{S}(\mathbf{p}_{Ci})$	surface contact
$\dot{\mathbf{p}}_{Ci}(t \in T_C) = \mathbf{0}$	no slip condition
$\mathbf{F}_{Ci}(t \in T_C) \in \mathcal{F}(\mathbf{F}_{Ci}, \mathbf{n}_S, \mu)$	friction cone
otherwise:	
$\mathbf{F}_{Ci}(t \notin T_C) = \mathbf{0}$	no contact force

Herein the double-integrator relation from  $\dot{\boldsymbol{\nu}}(t)$  to  $\mathbf{q}(t)$  can be expressed through the following state-space representation:

$$\dot{\mathbf{x}}(t) = \begin{bmatrix} \mathbf{0} & \hat{\mathbf{S}} \\ \mathbf{0} & \mathbf{0} \end{bmatrix} \mathbf{x}(t) + \mathbf{f}_{\text{quat}}(\mathbf{x}(t)) + \begin{bmatrix} \mathbf{0} & \mathbf{0} \\ \mathbf{I} & \mathbf{0} \end{bmatrix} \mathbf{u}(t) \quad (8)$$

where  $\mathbf{f}_{\text{quat}}(\mathbf{x})$  represents the quaternion propagation in (3), while the selection matrix  $\hat{\mathbf{S}}$  is given by:

$$\hat{\mathbf{S}} = [\mathbf{I}_{3 \times (n+n_u)} \quad \mathbf{0}_{4 \times (n+n_u)} \quad \mathbf{I}_{n \times (n+n_u)}]^T \quad (9)$$

When the robot is establishing contact with a surface  $\mathcal{S}$ , constraints on contact positions, velocities and forces must be simultaneously enforced. To this end, the following constraint:

$$\mathbf{p}_{Ci}(\mathbf{q}) \in \mathcal{S}(\mathbf{p}_{Ci}(\mathbf{q})) \quad (10)$$

ensures that the  $i$ -th contact point lays on the surface  $\mathcal{S}$ . In the simple planar case, the surface equation is given by:

$$\mathcal{S}(\mathbf{p}_{Ci}(\mathbf{q})) : \mathbf{n}_S^T \mathbf{p}_{Ci} + d = 0 \quad (11)$$

being  $\mathbf{n}_S = [a \ b \ c]^T \in \mathbb{R}^3$  the surface normal, with  $a, b, c, d \in \mathbb{R}$ . We also need to ensure that contact points do not slip, i.e.:

$$\dot{\mathbf{p}}_{Ci}(\mathbf{q}, \boldsymbol{\nu}) = \mathbf{J}_{Ci} \boldsymbol{\nu} = \mathbf{0} \quad (12)$$

In order to further encode the impact of the surface orientation on contact forces, friction constraints must be incorporated. Being  $\mathbf{F}_{Ci}^n \in \mathbb{R}^3$  and  $\mathbf{F}_{Ci}^t \in \mathbb{R}^3$ , the normal and tangential component of the contact force at the  $i$ -th contact point:

$$\mathbf{F}_{Ci}^n = (\mathbf{F}_{Ci} \cdot \mathbf{n}_S) \mathbf{n}_S \quad (13a)$$

$$\mathbf{F}_{Ci}^t = \mathbf{F}_{Ci} - (\mathbf{F}_{Ci} \cdot \mathbf{n}_S) \mathbf{n}_S \quad (13b)$$

the  $i$ -th point contact remains in rest contact mode if  $\mathbf{F}_{Ci}$  lies inside the friction cone directed by  $\mathbf{n}_S$ , i.e.:

$$\mathcal{F}(\mathbf{F}_{Ci}, \mathbf{n}_S, \mu) := \begin{cases} \mathbf{F}_{Ci} \cdot \mathbf{n}_S > F_{\text{thr}} \\ \|\mathbf{F}_{Ci}^t\|_2 \leq \mu(\mathbf{F}_{Ci} \cdot \mathbf{n}_S) \end{cases} \quad (14)$$

where  $\mu$  is the Coulomb friction coefficient, while  $F_{\text{thr}} \geq 0$  is a scalar force threshold. The Euclidean norm  $\|\cdot\|_2$  models Coulomb friction cones with circular section. The under-actuation constraint is implemented according to (5a) by denoting with  $\boldsymbol{\tau}_u \in \mathbb{R}^{n_u-1}$  the under-actuated torques, i.e.:

$$\boldsymbol{\tau}_u = \mathbf{B}_u \dot{\boldsymbol{\nu}} + \mathbf{h}_u - \mathbf{J}_{C,u}^T \mathbf{F}_C \quad (15)$$

Similarly, torque bounds are imposed on the actuated torques  $\boldsymbol{\tau} \in \mathbb{R}^n$ , whose expression can be retrieved from (5b):

$$\boldsymbol{\tau} = \mathbf{B}_a \dot{\boldsymbol{\nu}} + \mathbf{h}_a - \mathbf{J}_{C,a}^T \mathbf{F}_C \quad (16)$$

In order to perform a Direct Multiple Shooting (DMS) transcription [17] of (7) into a Nonlinear Program (NLP) that can be solved by off-the-shelf solvers [18], let us consider a number of shooting intervals  $N_s$ , which discretize the control horizon. The state variable and control vector at the  $k$ -th shooting interval,  $\mathbf{x}_k$  and  $\mathbf{u}_k$  respectively, are denoted as:

$$\mathbf{x}_k = [\mathbf{q}_k^T \quad \boldsymbol{\nu}_k^T]^T \quad (17a)$$

$$\mathbf{u}_k = [\dot{\boldsymbol{\nu}}_k^T \quad \mathbf{F}_{C,k}^T]^T \quad (17b)$$

We hereafter assume a piece-wise constant control parametrization along each shooting interval. The  $N_s + 1$  states are collected in the state vector  $\mathbf{X}$ :

$$\mathbf{X} = [\mathbf{x}_0^T, \mathbf{x}_1^T, \dots, \mathbf{x}_{N_s}^T]^T \quad (18)$$

and the  $N_s$  controls in the control vector  $\mathbf{U}$ :

$$\mathbf{U} = [\mathbf{u}_0^T, \mathbf{u}_1^T, \dots, \mathbf{u}_{N_s-1}^T]^T \quad (19)$$

In agreement with DMS, a *continuity condition* needs to be further satisfied:  $\mathbf{s}(\mathbf{x}_k, \mathbf{u}_k) - \mathbf{x}_{k+1} = \mathbf{0}$ . Here the function  $\mathbf{s}(\mathbf{x}_k, \mathbf{u}_k)$  is used to simulate the double integrator dynamics in (8) over one shooting interval. We additionally leave the solver free to decide the optimal step size for each shooting interval, introducing the step size variable  $dt_k \in \mathbb{R}^+$  in the control vector:

$$\mathbf{u}_k = [\dot{\boldsymbol{\nu}}_k^T \quad \mathbf{F}_{C,k}^T \quad dt_k]^T, \quad (20)$$

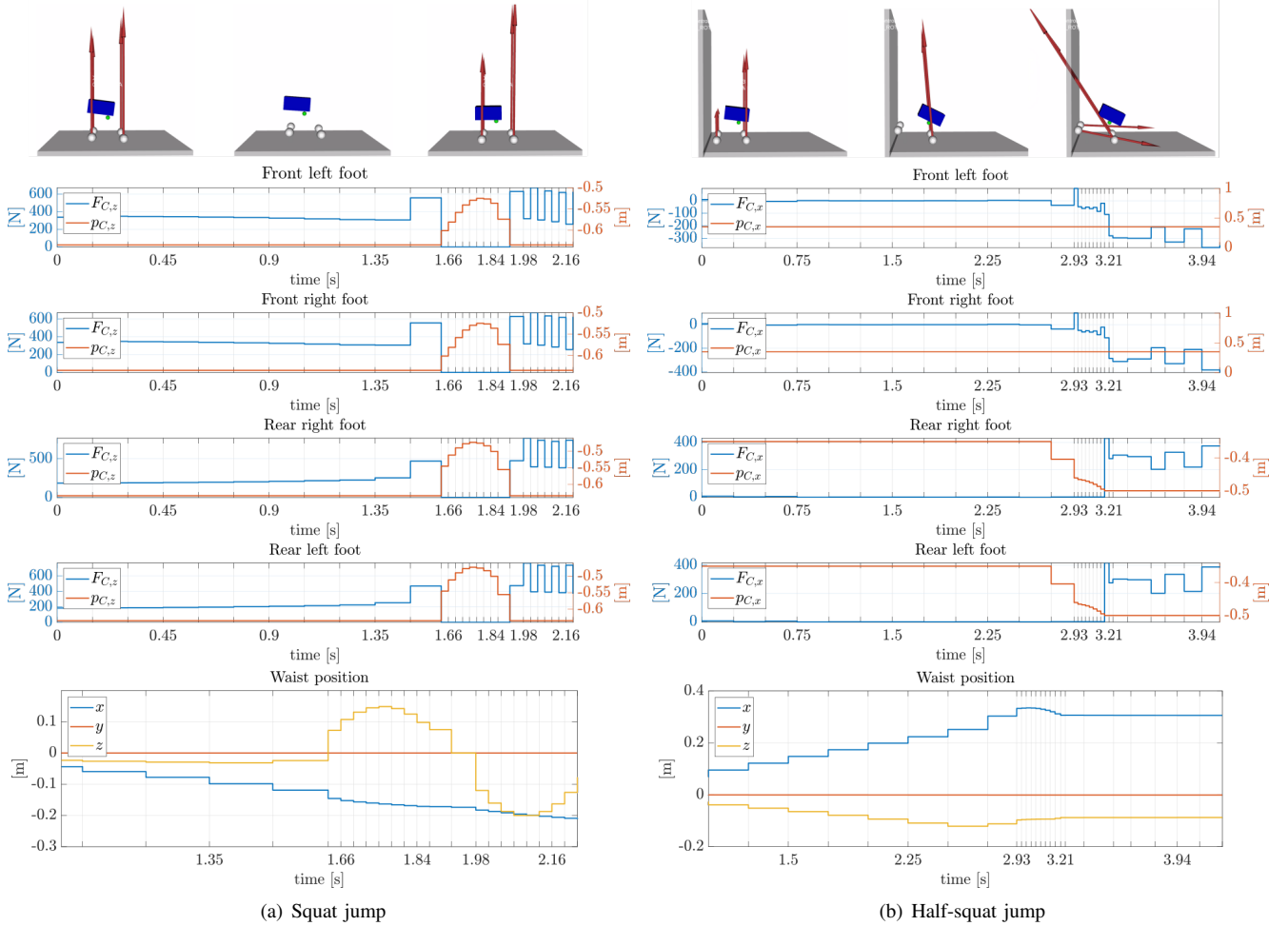


Fig. 3. Snapshots of the produced motion in rviz ROS with visualization of contact forces (upper snapshots) and time histories of contact forces, feet positions and waist position (lower plots) for the squat jump (left side) and the half-squat jump (right side) planned agile actions.

together with the bound:  $dt \leq dt_k \leq \bar{dt}$ . Finally, we adopted a linearized version of friction cones which, in our experience, is easier to handle for the solver.

#### D. Planned Agile Actions

Building upon the OCP in (7), we hereafter address the planning problem of a set of agile lower-body actions, consisting in two types of squat jumps. The related NLPs have been implemented using CasADi [19] and Pinocchio [20]<sup>1</sup>. The planned trajectories are then conveniently interpolated using the integrator function  $s(\cdot)$  with fixed step-size of  $1 \cdot 10^{-3}s$  and replayed on the robot in the online stage, see Fig. 1.

1) *Squat jump*: The robot is initially in contact with the ground, while its goal is to reach a target floating-base position  $\bar{p}_u \in \mathbb{R}^3$  displaced vertically along the  $z$ -axis. Since the control horizon comprises also the landing phase, we denote  $N_T$  as the take-off interval and  $N_L$  as the landing

interval, with:  $N_s = 30$ ,  $N_T = 10$  and  $N_L = 20$ . In order to give the possibility to the solver to determine the duration of each phase, the control vector comprises the step-size variable within the following bounds:  $dt_k = 0.03s$  and  $\bar{dt}_k = 0.25s$ . The following piece-wise cost function has been considered:

$$\begin{aligned}
 F(\mathbf{X}, \mathbf{U}) = & \sum_{k=N_T+1}^{N_L} \left( \gamma_\nu \boldsymbol{\nu}_k^T \boldsymbol{\nu}_k + \gamma_{p_u} (p_{u,k}^{[z]} - \bar{p}_u^{[z]})^2 \right) + \\
 & + \sum_{k=N_T+1}^{N_s} \gamma_{\dot{q}_c} \dot{\mathbf{q}}_{C,k}^T \dot{\mathbf{q}}_{C,k} + \sum_{k=N_L+1}^{N_s-2} \gamma_{\dot{F}_C} \dot{\mathbf{F}}_{C,k}^T \dot{\mathbf{F}}_{C,k} + \sum_{k=0}^{N_s-2} \gamma_{\dot{\nu}} \dot{\boldsymbol{\nu}}_k^T \dot{\boldsymbol{\nu}}_k
 \end{aligned} \quad (21)$$

with  $\gamma_{p_u} = 50$ ,  $\gamma_{\dot{q}_a} = 1$ ,  $\gamma_{\dot{F}_C} = 1$  and  $\gamma_{\dot{\nu}} = 10^{-3}$ . We first penalize the tracking of a target floating-base position along the  $z$ -axis during the flight phase only, i.e. between the take-off and the landing shooting interval. The second term in (21) minimizes the velocity of the actuated joints during the flight phase, while the third and last terms minimize the derivative of contact forces ( $\dot{\mathbf{F}}_{C,k} \approx \mathbf{F}_{C,k+1} - \mathbf{F}_{C,k}$ ) and of accelerations ( $\dot{\boldsymbol{\nu}}_k \approx \boldsymbol{\nu}_{k+1} - \boldsymbol{\nu}_k$ ), respectively, in order to smooth the control actions. Snapshots of the resulting motion and time

<sup>1</sup>Two software packages have been developed to this end: the *casadi\_kin\_dyn* library ([https://github.com/ADVRHumanoids/casadi\\_kin\\_dyn](https://github.com/ADVRHumanoids/casadi_kin_dyn)) and the *Horizon* library (<https://github.com/ADVRHumanoids/Horizon>)

histories of relevant quantities are depicted in Fig. 3(a) (these results are also illustrated in the accompanying video). Due to the introduced offset on the waist mass location (modeling the presence of the upper-body), the robot waist moves backward before jumping, so that contact forces are equally distributed. Note also how the solver adapts the step-size.

2) *Half-squat jump*: Inspired by the pushing task in [15], where CENTAURO contacts a wall with its rear feet in order to push a heavy object, we set up an OCP in which the robot, initially in contact with the ground  $\mathcal{S}_1$ , has to simultaneously lift and put its rear feet on a vertical surface  $\mathcal{S}_2$  pivoting on its front feet, in a so-called “half-squat jump” manoeuvre. The following parameter have been selected:  $N_s = 30$ ,  $N_T = 10$  and  $N_L = 20$ ,  $\underline{dt}_k = 0.03s$ ,  $\overline{dt}_k = 0.25s$ . The cost function in (21) has been employed, with same weights, now penalizing the tracking of the initial floating-base pose. Snapshots of the resulting motion and time histories of relevant quantities are depicted in Fig. 3(b). The robot waist moves towards the front feet in order to be able to lift the rear legs and consequently establish contact with the vertical surface.

#### IV. UPPER-BODY STABILIZERS

We here present three different feedback strategies that exploit upper-body motion to maintain balance.

##### A. Raibert-Like Postural Task

In the work of Raibert on the one-legged hopper [6], body posture control on ground is obtained by setting the torque between the leg and the body to be proportional to the body angle. As a result, the balance arm, acting as fly wheel, spins in the direction of falling in order to stabilize the system posture. Applying a similar control approach to the upper-body of a humanoid, the following postural task can be introduced:

$$\mathcal{T}_{\text{Posture-Raibert}} : \mathbf{S}_{\text{ub}} \mathbf{q}_{d,k+1} = \mathbf{S}_{\text{ub}} \mathbf{q}_{d,k} + \mathbf{\Gamma} \boldsymbol{\omega}_{\text{imu}} \quad (22)$$

where  $\mathbf{q}_d \in \mathbb{R}^n$  is the desired robot posture (initialized in the homing configuration), the matrix  $\mathbf{S}_{\text{ub}} \in \mathbb{R}^{n \times n}$  enables the motion of a subset of the upper-body joints,  $\boldsymbol{\omega}_{\text{imu}} \in \mathbb{R}^3$  is the measured IMU angular velocity, while  $\mathbf{\Gamma} \in \mathbb{R}^{n \times 3}$  is a gain matrix. The considered SoT can be written using the Math of Task (MoT) formalism [21] as follows:

$$\left( \left( \sum_i \text{Pelvis} \mathcal{T}_{\text{Foot}_i}^{\text{[XYZ]}} \right) / \right) \ll \left( \mathcal{C}_{\text{Lims}}^{\text{Pos.}} + \mathcal{C}_{\text{Lims}}^{\text{Vel.}} \right), \quad (23)$$

Note that the first layer is responsible for the tracking of the planned lower-body trajectories.

##### B. Angular Momentum Task

An alternative stabilizing strategy consists in controlling the system’s centroidal momentum [22] to maintain balance through emergent arm motions, thus without authoring any upper-body motion, as in Sec. IV-A. Let  $\mathbf{h} \in \mathbb{R}^6$  be the rate of change of the system centroidal momentum:

$$\mathbf{h} = \mathbf{A}(\mathbf{q}) \dot{\mathbf{q}} \quad (24)$$

where  $\mathbf{A}(\mathbf{q}) \in \mathbb{R}^{6 \times (n+6)}$  is the centroidal momentum matrix. The centroidal momentum  $\mathbf{h} = [\mathbf{h}_{\text{lin}}^T \ \mathbf{h}_{\text{ang}}^T]^T$  is a spatial

quantity comprised of the system’s net linear momentum  $\mathbf{h}_{\text{lin}} \in \mathbb{R}^3$  and angular momentum  $\mathbf{h}_{\text{ang}} \in \mathbb{R}^3$  about the CoM.

Similarly to [5], in order to maintain balance through emergent arm motions, the following angular momentum task  $\mathcal{T}_{\text{AngMom}}$  can effectively provide a dampening of any excess angular momentum:

$$\mathcal{T}_{\text{AngMom}} : \mathbf{h}_{\text{ang}, d} = 0 \quad (25)$$

The resulting SoT can be written as follows:

$$\left( \left( \sum_i \text{Pelvis} \mathcal{T}_{\text{Foot}_i}^{\text{[XYZ]}} \right) / \right) \ll \left( \mathcal{C}_{\text{Lims}}^{\text{Pos.}} + \mathcal{C}_{\text{Lims}}^{\text{Vel.}} \right), \quad (26)$$

where the task  $\text{World} \mathcal{T}_{\text{Pelvis}}$  is used to conveniently incorporate the IMU feedback as follows:

$$\text{World} \mathcal{T}_{\text{Pelvis}} : \boldsymbol{\omega}_{\text{fb}, d} = -\boldsymbol{\omega}_{\text{imu}} \quad (27)$$

##### C. OCP Postural Task

Building upon the idea of treating the upper-body of a humanoid as a fly wheel in order to produce enough angular momentum to maintain balance, a dedicated OCP can be designed to produce a *periodic* joint-space trajectory which maximizes the angular momentum along the tilting axis. The optimization is done on the fixed-based single-arm model of the robot, with  $\mathbf{x} = [\mathbf{q}^T \ \dot{\mathbf{q}}^T]^T$  and  $\mathbf{u} = \ddot{\mathbf{q}}$ . With abuse of notation here  $\mathbf{q} \in \mathbb{R}^{n_{\text{arm}}}$  is the single arm joint vector. Some of the constraints in the optimization are:

- Same initial and final state, in order to produce a periodic trajectory. Note that, the the solver is let free to choose the arm’s initial configuration.
- Joint position, velocity and torque bounds.
- Work-space constraints on the end-effector Cartesian position, to prevent self-collisions.

The problem can be set up as DMS transcription with  $N_s$  shooting intervals over a normalized time horizon, where the following cost function has been considered:

$$F(\mathbf{X}, \mathbf{U}) = \sum_{k=0}^{N_s} \left( \gamma \mathbf{h}_{\text{ang}} (\mathbf{h}_{\text{ang},k} - \mathbf{h}_d) + \gamma \dot{\mathbf{q}}_k^T \dot{\mathbf{q}}_k \right) \quad (28)$$

in order to maximize the angular momentum e.g. along the  $y$ -axis. Similarly to the fly wheel control in [6], the planned joint-space trajectory  $\mathbf{q}^* \in \mathbb{R}^{n_{\text{arm}} \times N_s}$  can be then replayed forward and backward on each robot arm with a velocity scaling proportional to the IMU feedback. In order to do so, by considering an equivalent SoT to the one in (23), an upper-body postural task  $\mathcal{T}_{\text{Posture-OCP}}$  is designed as follows:

$$\mathcal{T}_{\text{Posture-OCP}} : \mathbf{q}_d = \mathbf{q}_k^* + N_s (\tau_{k+1} - k/N_s) (\mathbf{q}_{k+1}^* - \mathbf{q}_k^*) \quad (29)$$

where the scaling factor  $\tau_{k+1} \in [0, 1]$  is proportional to the IMU angular velocity controlled component, e.g. the pitch:

$$\tau_{k+1} = \tau_k + \gamma_\tau \omega_{\text{imu}}^{[P]} \quad (30)$$

being the sample  $k \in \mathbb{R}$  given by:  $k = \lfloor N_s \cdot \tau_{k+1} \rfloor$ .

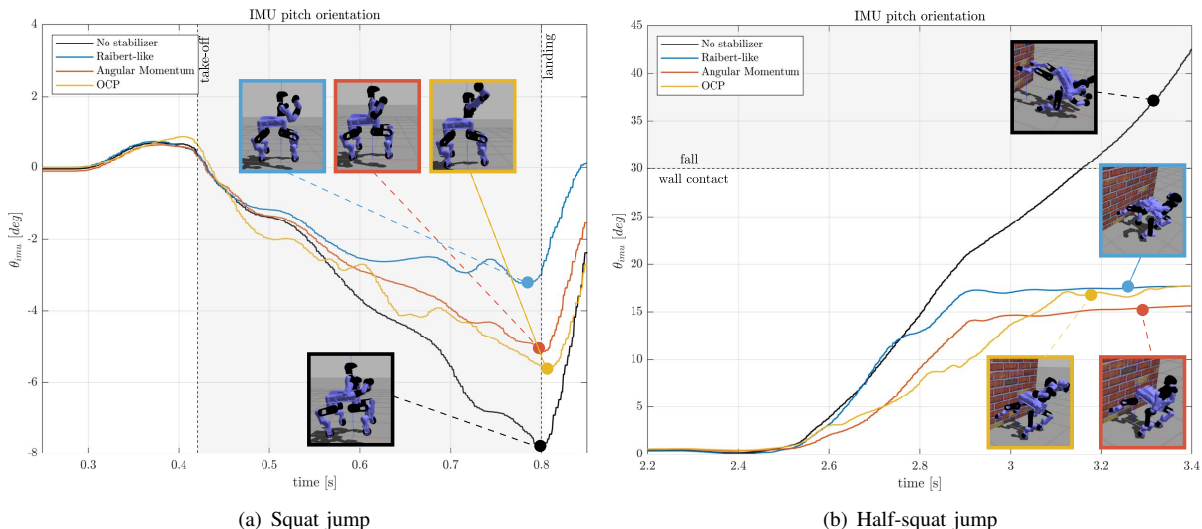


Fig. 4. Time histories of the IMU pitch orientation and snapshots from Gazebo simulations of the squat jump (left side) and the half-squat jump (right side) planned agile actions, with and without (black solid lines) the proposed upper-body stabilizing strategies.

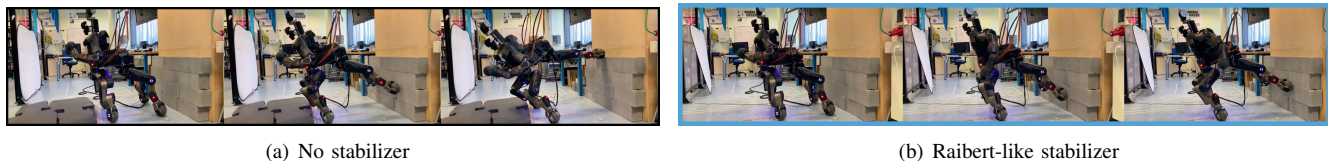


Fig. 5. Snapshots from performed half-squat jumps experiments with no stabilizing action (left side) and employin with the proposed Raibert-like postural task (right side). The arms' motion effectively prevents the robot from tilting excessively, thus allowing to establish a steady contact with the wall.

## V. VALIDATION

In order to first compare the performance of the proposed upper-body stabilizers, we set up a simulation benchmark scenario in Gazebo using the CENTAURO robot [14] to perform the planned agile actions. CENTAURO is a 39 DoF hybrid wheeled-legged quadruped equipped with a bimanual humanoid upper-body, and has a weight of 92 kg. The robot is fully torque-controlled with direct sensing of the link-side torque. CENTAURO is powered by the *XBotCore* middleware [23], while the *CartesIO* framework [24], which relies on the hierarchical IK library *OpenSoT* [21], is responsible for Cartesian control. Three separate ROS nodes running at 1 kHz are responsible for the replay of the planned lower-body trajectories, the HIK managed by *CartesIO*, and the contact force distribution among the lower-body contact points, respectively. The joint-level controller runs at 2 kHz. Snapshots and time histories of the IMU pitch orientation are shown in Fig. 3. These results are illustrated in the provided supplementary video. Performing the squat jump without upper-body stabilization results in a notable tilt of the robot waist. Similarly, in the half-squat jump, the absence of upper-body stabilization results in an excessive tilt of the robot, eventually causing it to fall without accomplishing the task. In order to effectively mitigate the tilt rotation measured by  $\omega_{imu}^{[P]}$ , the shoulder pitch and elbow pitch joints have been enabled through  $S_{ub}$  in  $\mathcal{T}_{Posture-Raibert}$ , see (22), while the motion of the shoulder joints and the

elbow joints is engaged in  $\mathcal{T}_{AngMom}$ . All the arm joints have been considered in  $\mathcal{T}_{Posture-OCP}$ . Based on the benchmark results, trading-off controller performance against number of parameters to tune and complexity of motion, i.e. number of enabled joints, the Raibert-like stabilizer stands out as the most suitable algorithm to perform experiments on the real robotic platform. In this respect, note that, although self-collisions are not inherently prevented, no collisions occurred in the performed agile actions for our choice of parameters. Due to high peak torques involved in the squat jump and battery current limitations, experimental validation has been successfully performed on the half-squat jump task employing the Raibert-like stabilizing action, see Fig. 5.

## VI. CONCLUSIONS

Aiming at performing agile actions with a centaur-type torque-controlled humanoid, this paper has presented a decoupled control architecture which meets the computational and implementation requirements to achieve a real demonstrator. Lower-body motion primitives are generated through optimal control in an offline stage, based on a simplified kinematic model. The planned lower-body trajectories are then replayed on the robot, in the online stage, using three different upper-body stabilizing strategies to maintain balance. The stabilizers' performance has been compared in two types of simulated jumps, while experimental validation has been performed on a half-squat jump using CENTAURO.

## REFERENCES

- [1] K. Nagasaka, Y. Kuroki, S. Suzuki, Y. Itoh, and J. Yamaguchi, "Integrated motion control for walking, jumping and running on a small bipedal entertainment robot," in *IEEE International Conference on Robotics and Automation*, vol. 4, 2004, pp. 3189–3194.
- [2] C. Gehring, S. Coros, M. Hutter, *et al.*, "Practice makes perfect: An optimization-based approach to controlling agile motions for a quadruped robot," *IEEE Robotics & Automation Magazine*, vol. 23, no. 1, pp. 34–43, 2016.
- [3] M. Hutter, C. Gehring, *et al.*, "Anymal-toward legged robots for harsh environments," *Advanced Robotics*, vol. 31, no. 17, pp. 918–931, 2017.
- [4] B. Katz, J. Di Carlo, and S. Kim, "Mini cheetah: A platform for pushing the limits of dynamic quadruped control," in *IEEE International Conference on Robotics and Automation*, 2019, pp. 6295–6301.
- [5] P. M. Wensing *et al.*, "Generation of dynamic humanoid behaviors through task-space control with conic optimization," in *IEEE International Conference on Robotics and Automation*, 2013, pp. 3103–3109.
- [6] M. H. Raibert, *Legged robots that balance*. MIT press, 1986.
- [7] R. Niyama, A. Nagakubo, *et al.*, "Mowgli: A bipedal jumping and landing robot with an artificial musculoskeletal system," in *IEEE International Conference on Robotics and Automation*, 2007, pp. 2546–2551.
- [8] H. Dai, A. Valenzuela, and R. Tedrake, "Whole-body motion planning with centroidal dynamics and full kinematics," in *IEEE-RAS International Conference on Humanoid Robots*, 2014, pp. 295–302.
- [9] S. Sakka and K. Yokoi, "Humanoid vertical jumping based on force feedback and inertial forces optimization," in *IEEE International Conference on Robotics and Automation*, 2005, pp. 3752–3757.
- [10] F. Bergonti, L. Fiorio, and D. Pucci, "Torque and velocity controllers to perform jumps with a humanoid robot: theory and implementation on the iCub robot," in *IEEE International Conference on Robotics and Automation*, 2019, pp. 3712–3718.
- [11] S. Seok, *et al.*, "Design principles for highly efficient quadrupeds and implementation on the mit cheetah robot," in *IEEE International Conference on Robotics and Automation*, 2013, pp. 3307–3312.
- [12] H.-W. Park, P. M. Wensing, S. Kim, *et al.*, "Online planning for autonomous running jumps over obstacles in high-speed quadrupeds," 2015.
- [13] G. Kenneally, A. De, and D. E. Koditschek, "Design principles for a family of direct-drive legged robots," *IEEE Robotics and Automation Letters*, vol. 1, no. 2, pp. 900–907, 2016.
- [14] N. Kashiri, L. Baccelliere, L. Muratore, *et al.*, "CENTAURO: A Hybrid Locomotion and High Power Resilient Manipulation Platform," *IEEE Robotics and Automation Letters*, vol. 4, no. 2, pp. 1595–1602, 2019.
- [15] M. Parigi Polverini, A. Laurenzi, E. Mingo Hoffman, F. Ruscelli, and N. G. Tsagarakis, "Multi-Contact Heavy Object Pushing with a Centaur-Type Humanoid Robot: Planning and Control for a Real Demonstrator," *IEEE Robotics and Automation Letters*, vol. 5, no. 2, pp. 859–866, 2020.
- [16] B. Graf, "Quaternions and dynamics," 2008.
- [17] M. Diehl, H. G. Bock, H. Diedam, and P.-B. Wieber, "Fast direct multiple shooting algorithms for optimal robot control," in *Fast motions in biomechanics and robotics*. Springer, 2006, pp. 65–93.
- [18] A. Wächter and L. T. Biegler, "On the implementation of an interior-point filter line-search algorithm for large-scale nonlinear programming," *Mathematical programming*, vol. 106, no. 1, pp. 25–57, 2006.
- [19] J. A. E. Andersson, J. Gillis, G. Horn, *et al.*, "CasADi – A software framework for nonlinear optimization and optimal control," *Mathematical Programming Computation*, vol. 11, no. 1, pp. 1–36, 2019.
- [20] J. Carpentier, F. Valenza, N. Mansard, *et al.*, "Pinocchio: fast forward and inverse dynamics for poly-articulated systems," <https://stack-of-tasks.github.io/pinocchio>, 2015–2019.
- [21] E. Mingo Hoffman, A. Rocchi, A. Laurenzi, and others., "Robot Control for Dummies: Insights and Examples using OpenSoT," in *IEEE-RAS International Conference on Humanoid Robots*, 2017, pp. 736–741.
- [22] D. E. Orin, A. Goswami, *et al.*, "Centroidal dynamics of a humanoid robot," *Autonomous Robots*, vol. 35, no. 2-3, pp. 161–176, 2013.
- [23] L. Muratore, A. Laurenzi, E. Mingo Hoffman, *et al.*, "Xbotcore: A real-time cross-robot software platform," in *IEEE International Conference on Robotic Computing (IRC)*, 2017, pp. 77–80.
- [24] A. Laurenzi, E. M. Hoffman, *et al.*, "CartesI/O: A ROS based real-time capable cartesian control framework," in *IEEE International Conference on Robotics and Automation*, 2019, pp. 591–596.